

Enhanced reflection chiroptical effect of planar anisotropic chiral metamaterials placed on the interface of two media*

Xiu Yang(杨秀)¹, Tao Wei(魏涛)², Feiliang Chen(陈飞良)³, Fuhua Gao(高福华)^{1,4},
Jinglei Du(杜惊雷)^{1,4,†}, and Yidong Hou(侯宜栋)^{1,‡}

¹College of Physics, Sichuan University, Chengdu 610065, China

²School of Medical Information Engineering, Jining Medical University, Jining 272067, China

³Microsystem & Terahertz Research Center of CAEP, China Academy of Engineering Physics, Chengdu 610299, China

⁴High Energy Density Physics of the Ministry of Education Key Laboratory, Sichuan University, Chengdu 610064, China

(Received 6 April 2020; revised manuscript received 5 June 2020; accepted manuscript online 18 June 2020)

The strong chiroptical effect is highly desirable and has a wide range of applications in biosensing, chiral catalysis, polarization tuning, and chiral photo detection. In this work, we find a simple method to enhance the reflection circular dichroism (CD_R) by placing the planar anisotropic chiral metamaterials (i.e., Z-shaped PACMs) on the interface of two media (i.e., Z-PCMI) with a large refractive index difference. The maximum reflection CD_R from the complex system can reach about 0.840 when the refractive index is set as $n_{top} = 4.0$ and $n_{bottom} = 1.49$, which is approximately three times larger than that of placing the Z-shaped PACMs directly on the substrate (i.e., Z-PCMS). While the minimum reflection CD_R is 0.157 when the refractive index is set as $n_{top} = 1.0$ and $n_{bottom} = 1.49$. So we can get a large available range of reflection CD_R from -0.840 to -0.157 . Meanwhile, the transmission CD_T remains unchanged with the refractive index n_{top} increment. Our in-depth research indicates that the large reflection CD_R is derived from the difference of non-conversion components of the planar anisotropic chiral metamaterials' reflection matrices. In short, we provide a simple and practical method to enhance the chiroptical effect by changing the refractive index difference between two media without having to design a complex chiral structure.

Keywords: chiroptical effect, chiral metamaterials, refractive index

PACS: 81.05.Xj, 42.25.Bs, 78.20.Ci, 42.25.-p

DOI: 10.1088/1674-1056/ab9def

1. Introduction

Recently, plasmonic chiral metamaterials (PCMs) composed by electric or magnetic resonators have attracted a great amount of attention for their large chiroptical effect and wide applications. The strong chiral resonance of the PCMs results from the matching of space structure and electromagnetic wave, which leads to two important chiroptical effects, including the optical activity (OA), which means the capacity to induce the rotation of the polarization plane.^[1,2] The circular dichroism (CD), i.e., differential absorption of left-hand (LCP) and right-hand (RCP) circularly polarization lights,^[2,3] existing in nature like DNA and protein molecules,^[4] has a widespread application in practical fields. Meanwhile, the large CD of the PCMs can reach almost 1, which is about 1000 times larger than that from nature chiral molecules.^[5-7] These large chiroptical effects of PCMs are used to control the polarization state of light,^[8-10] biosensing,^[11,12] and also enable many fascinating physical effects, such as negative refraction index,^[13-15] repulsive Casimir effect,^[16,17] circular conversion dichroism,^[18,19] and unusual spin Hall effect.^[20,21]

A strong chiroptical effect is highly desirable for practical applications. Due to spatial matching, the artificial chiral structure has a large chiroptical effect. At present, there are many very well known artificial chiral structures, such as fish-shaped,^[22] Y-shaped resonator,^[23] split-ring-resonator,^[24-26] helix chiral structures,^[27] and twisted-arcs array structures.^[28] Depending on their spatial dimensions, the structures developed thus far can be either two-dimensional (2D or planar)^[29] or three-dimensional (3D).^[30,31] The 2D planar structure has a relatively simple spatial structure and has a stronger chiroptical effect compared to nature chiral molecules; while the 3D structure has a relatively complex spatial structure, they can feel the 3D electromagnetic field distortion along the light propagation direction, so their chiroptical response is very strong. Because the optical activity of these structure relies primarily on the precise geometrical arrangement of their constituent elements in a unit cell, electron beam lithography and direct laser writing have frequently been used for small-scale fabrication yet at high cost and time consumption. There are also relatively simple processing technologies to achieve the

*Project supported by the National Natural Science Foundation of China (Grant No. 11604227).

†Corresponding author. E-mail: dujl@scu.edu.cn

‡Corresponding author. E-mail: houyd@scu.edu.cn

structure, but the chiral response is small.

To date, a strong chiroptical effect is usually achieved by designing a new chiral structure. Lastly, a more general method to enhance the chiroptical effect through the micro-cavity interference effect has been found.^[32] We propose a high-performance active chiral metamaterial absorber (ACMA) composed by PACMs and a metal layer. Through in-deep theoretical analysis indicates that the circular conversion dichroism (CCD) from the PACMs plays a crucial role to achieve the active chiroptical effect. Numerical simulations demonstrate that the maximum reflection CD_R from the ACMA can reach about 0.882.^[33] In this work, we explore a new enhancement method by placing the Z-shaped PACMs on the interface of two media (i.e., Z-PCMI) with large refractive index differences. The large chiroptical effect is related to the refractive index difference of the two media. In simulations, the large range of reflection CD_R is from -0.840 to -0.157 , and the maximum reflection CD_R is close to the ideal value of 1. Further research indicates that the non-conversion components of the PACMs' reflection matrices play an important role to achieve the large chiroptical effect. In addition, the strong CD_R can be applied to various fields.

2. Theoretical model

The Z-PCMI is constructed by one layer of PACMs and two dielectric layers. The Jones matrix is used to characterize the chiral metamaterial, and its transmission matrix \hat{t}_{circ} and reflection matrix \hat{r}_{circ} are defined as^[34]

$$\hat{t}_{\text{circ}} = \begin{pmatrix} t_{++} & t_{+-} \\ t_{-+} & t_{--} \end{pmatrix}, \quad \hat{r}_{\text{circ}} = \begin{pmatrix} r_{++} & r_{+-} \\ r_{-+} & r_{--} \end{pmatrix}, \quad (1)$$

where $-$ and $+$ denote the LCP and RCP, respectively. The circular transmission/reflection coefficients can be written as t_{ij}/r_{ij} , where i and j denote the polarized states of the output and incident lights, respectively. In order to extract the circular transmission and reflection coefficients, the transmission and reflection coefficients for the linear polarization lights illuminate along $-z$ direction have been calculated firstly. The \hat{t}_{line} - and \hat{r}_{line} -matrix connects for linear polarization lights can be written as

$$\hat{t}_{\text{line}} = \begin{pmatrix} t_{xx} & t_{xy} \\ t_{yx} & t_{yy} \end{pmatrix}, \quad \hat{r}_{\text{line}} = \begin{pmatrix} r_{xx} & r_{xy} \\ r_{yx} & r_{yy} \end{pmatrix}, \quad (2)$$

where x and y denote the X and Y -polarization lights, respectively. Then the circular transmission and reflection coefficients, i.e., \hat{t}_{circ} and \hat{r}_{circ} , can be written as^[35]

$$\begin{aligned} \hat{t}_{\text{circ}} &= \begin{pmatrix} t_{++} & t_{+-} \\ t_{-+} & t_{--} \end{pmatrix} = \frac{1}{2} \begin{pmatrix} t_{xx} + t_{yy} + \sqrt{-1}(t_{xy} - t_{yx}) & t_{xx} - t_{yy} - \sqrt{-1}(t_{xy} + t_{yx}) \\ t_{xx} - t_{yy} + \sqrt{-1}(t_{xy} + t_{yx}) & t_{xx} + t_{yy} - \sqrt{-1}(t_{xy} - t_{yx}) \end{pmatrix}, \\ \hat{r}_{\text{circ}} &= \begin{pmatrix} r_{++} & r_{+-} \\ r_{-+} & r_{--} \end{pmatrix} = \frac{1}{2} \begin{pmatrix} r_{xx} - r_{yy} + \sqrt{-1}(r_{xy} + r_{yx}) & r_{xx} + r_{yy} - \sqrt{-1}(r_{xy} - r_{yx}) \\ r_{xx} + r_{yy} + \sqrt{-1}(r_{xy} - r_{yx}) & r_{xx} - r_{yy} - \sqrt{-1}(r_{xy} + r_{yx}) \end{pmatrix}. \end{aligned} \quad (3)$$

The transmissivity T_{ij} (the reflectivity R_{ij}) and the phase retardation $\varphi_{r,ij}$ ($\varphi_{r,ij}$) can be calculated by $T_{ij} = |t_{ij}|^2$ ($R_{ij} = |r_{ij}|^2$), and $\varphi_{t,ij} = \arg(t_{ij})$ ($\varphi_{r,ij} = \arg(r_{ij})$), respectively.

According to the basic definition, the CD_R can be calculated as

$$CD_R = \frac{R_+ - R_-}{R_+ + R_-}, \quad (4)$$

where $R_+ = R_{++} + R_{-+}$ and $R_- = R_{--} + R_{+-}$.

In general, for the ideal planar isotropic chiral media, there are no non-conversion parts in the reflection matrix, i.e., $r_{++} = r_{--} = 0$, and the conversion parts are equal to each other, i.e., $r_{+-} = r_{-+}$, indicating that no chiroptical effect is observed in the reflection. While for the ideal planar anisotropic chiral media, the conversion parts do not exist, i.e., $r_{+-} = r_{-+} = 0$, the chiroptical effect is derived from the difference of the non-conversion parts in the reflection coefficients, i.e., $r_{++} \neq r_{--}$. More discussion on the reflection matrices of planar isotropic chiral media and planar anisotropic media can be found in Refs. [36–39].

3. Results and discussion

Figure 1(a) shows the structure of the Z-PCMI, which is to place the Z-shaped PACMs on the interface of two media. The length and width for the wide and narrow parts of the Z-shaped PACMs are L_1 and W_1 , L_2 and W_2 , respectively. The thickness of the Z-shaped PACMs is h and the refractive indexes of the upper and lower dielectric media are n_{top} and n_{bottom} , respectively. For a comparative study, another Z-PCMS structure is shown in Fig. 1(b). It is to place the Z-shaped PACMs directly on the substrate. The parameters of the Z-PCMS are the same as those in Fig. 1(a), but there is no upper media. The finite difference time domain method (FDTD) is applied to numerical simulation. The periodic boundary is used in both X - and Y -directions and a perfect matching layer is used in the Z direction. The silver (Ag) is used as the nanostructure material and the optical constants of Ag are taken from the previously measured values.^[40] In order to extract the circular reflection and transmission and reflection coefficients, the transmission and reflection coefficients for linear polariza-

tion lights have been calculated firstly by analyzing the simulated datum from monitors in the reflection and transmission spaces.

The reflection coefficients of the two structures for the X - or Y -polarization light illumination along $-Z$ direction are calculated as shown in Figs. 1(c)–1(f). For planar anisotropic chiral media, the reflection matrix is a non-Hermitian matrix with equal off-diagonal elements, while the CCD is caused by the difference in magnitudes of the diagonal elements. For the Z-PCMS (i.e., $n_{\text{bottom}} = 1.0$), the conversion parts of the reflection coefficients are equal to each other, i.e., $R_{+-} = R_{-+}$, and the reflection CD_R is originated from the difference be-

tween R_{++} and R_{--} , which is about -0.292 at 578 nm. For the Z-PCMI, i.e., $n_{\text{top}} = 4.0$ and $n_{\text{bottom}} = 1.49$, a huge difference is observed from the non-conversion parts, i.e., R_{++} and R_{--} , especially near the wavelength of 1582 nm. This huge difference together with the near zero value reflectance of R_{+-} and R_{-+} leads to a large reflection CD_R about 0.840 , which is about 3 times larger than that from the Z-PCMS, while the minimum CD_R is about 0.227 , resulting in a large variation range from -0.840 to -0.227 . These results indicate that placing the PACMs on the interface of two media with a large reflection index difference will obviously enhance the reflection CD_R .

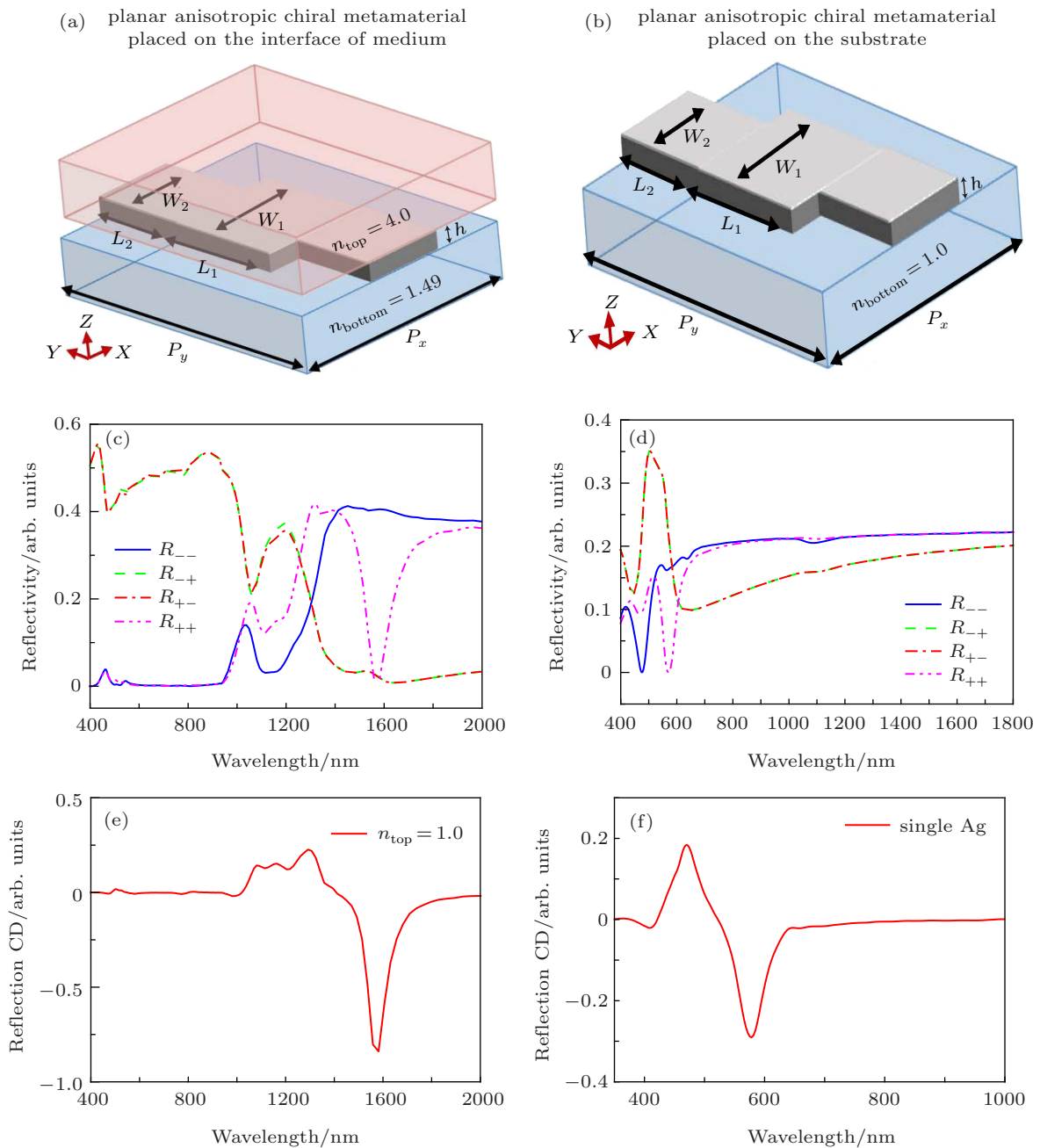


Fig. 1. Simulated reflection intensities of the Z-PCMI and Z-PCMS. (a) Schematic diagram of the Z-PCMI. The structure parameters are set as $w_1 = 115$ nm, $w_2 = 85$ nm, $L_1 = 125$ nm, $L_2 = 105$ nm, $P_x = 235$ nm, and $P_y = 335$ nm. The thickness h of the Z-shaped PACMs is 40 nm. (b) Schematic diagram of the Z-PCMS. (c)–(f) The simulated reflection intensities and CD_R of the Z-PCMI and Z-PCMS, respectively.

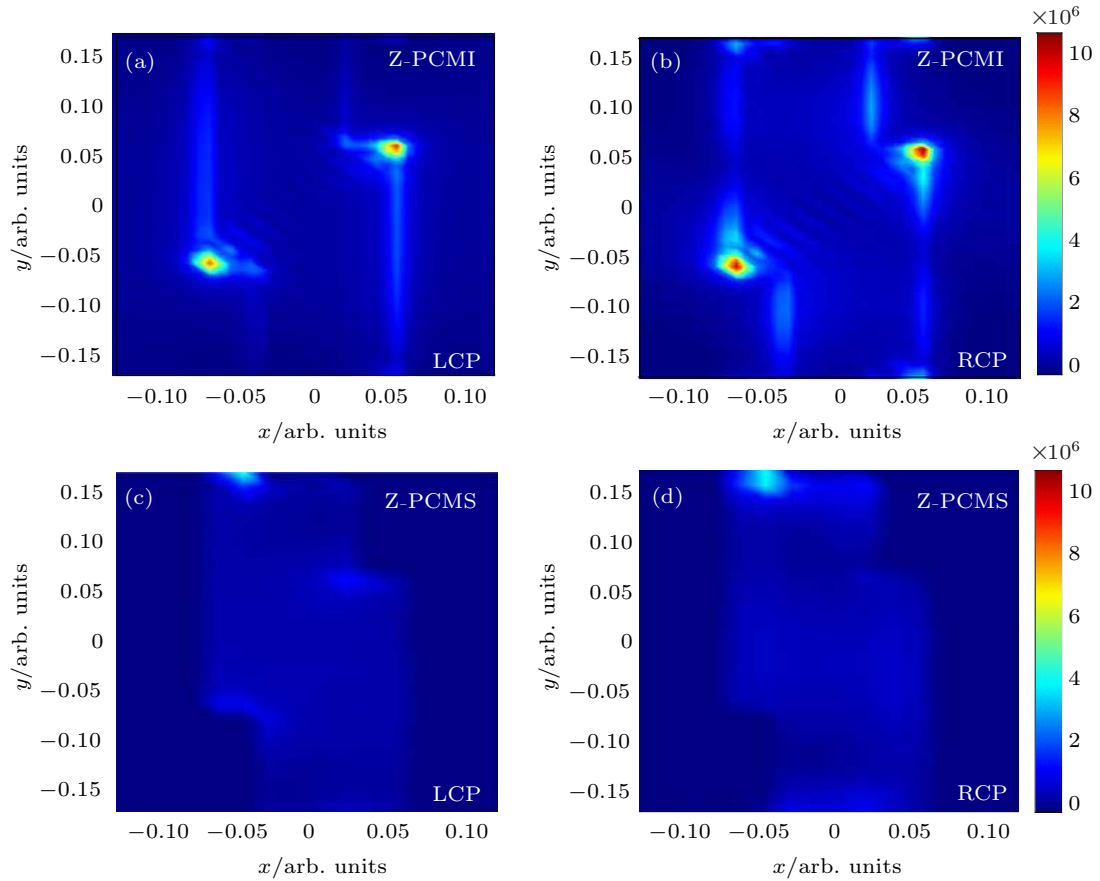


Fig. 2. The distribution of the electric field of the (a), (b) Z-PCMI and (c), (d) Z-PCMS at the resonant wavelengths of 1582 nm and 578 nm under the illumination of LCP and RCP.

In order to illustrate the resonance mode of the CD_R peak, the distributions of electric field (E) and electric charge (Q) of the Z-PCMI and Z-PCMS at the resonant wavelengths of 1582 nm and 578 nm are calculated under the illumination of LCP and RCP, as shown in Figs. 2 and 3. As shown in Figs. 2(a)–2(d), for the Z-PCMI, the two inflection points of the Z-shaped structure will excite strong electromagnetic modes and appear as hot spots. While for the Z-PCMS, the electric field is evenly distributed and there are no strong electric field hot spots. The electric field distribution of the two structures under the illumination of the LCP and RCP is the same except that a greater electric field intensity is formed in the Z-PCMI under the illumination of the RCP as shown in Figs. 2(a) and 2(b).

As shown in Figs. 3(a)–3(d), for the charge distribution of the Z-CMI and Z-PCMS, under the illumination of the LCP, the two structures have the same charge distribution with positive charge in the upper left and negative charge in the lower right. While under the illumination of RCP, the charge distribution of the two structures is more obvious with the negative charge in the upper right and the positive charge in the lower left. These results indicate that the Z-PCMI not only changes the electric field mode, but also shows a clearer charge distribution on the interface.

To better clarify the influence of resonance modes and structural parameters on CD peaks, we plot the reflection CD_R and transmission CD_T spectra of the Z-PCMI by changing the refractive index n_{top} as shown in Fig. 4. The refractive index of the top medium n_{top} increases from 1 to 4, while the refractive index of the lower medium n_{bottom} keeps at 1.49. The reflection CD_R and transmission CD_T of the Z-PCMI are obtained for the light illuminating along $-Z$ direction and $+Z$ direction as shown in Figs. 4(a)–4(d). As shown in Fig. 4(a), when the light illuminates along $-Z$ direction, the resonance wavelength red-shifts from 687 nm to 1582 nm and the reflection CD_R intensity gradually increases from 0.157 to 0.840 when the refractive index n_{top} increases from 1 to 4. When the light illuminates along $+Z$ direction, with the increase of the refraction index n_{top} , the reflection CD_R peak gradually decreases from 0.5 to 0.062 and redshifts as shown in Fig. 5(c). In contrast, the transmission CD_T changes a little with the increase of refractive index n_{top} and also redshifts as shown in Figs. 4(b) and 4(d). These results show that the reflection CD_R intensity of the Z-PCMI is significantly related to the refractive index difference of the two media, while the transmission CD_T intensity is not sensitive to the change of the refractive index.

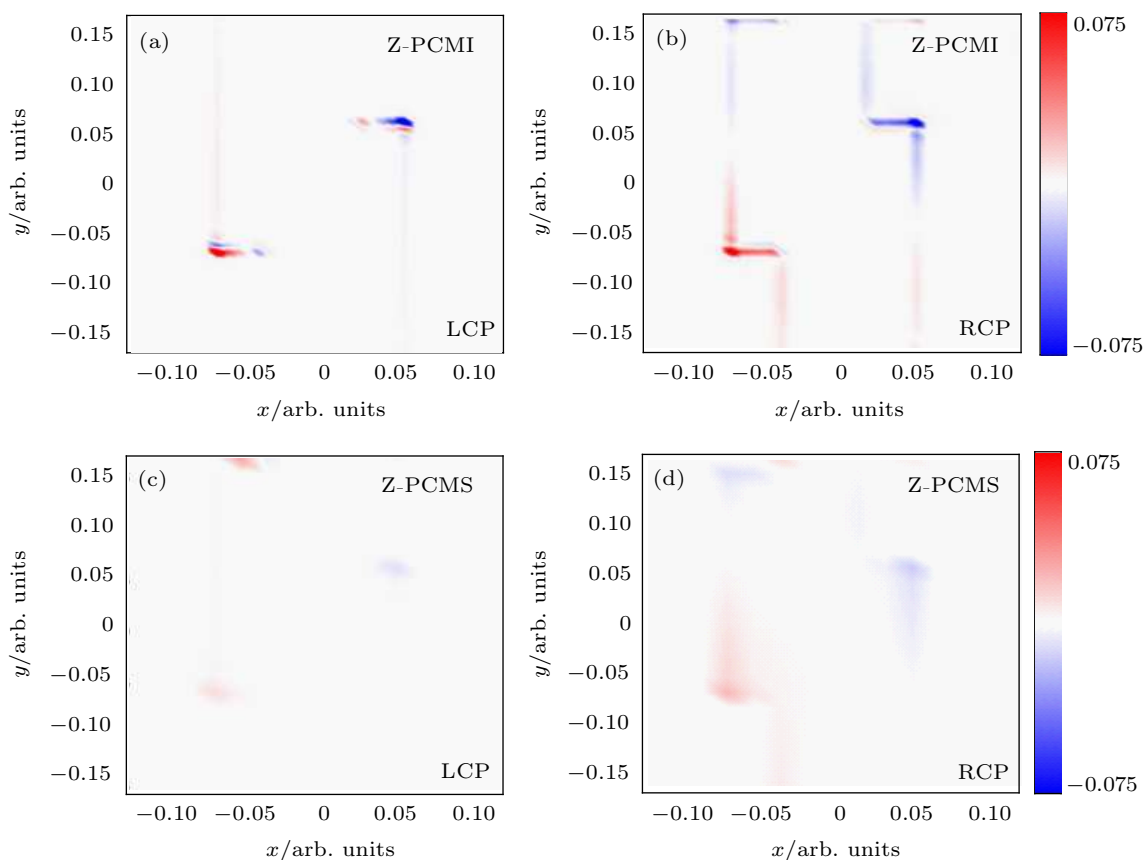


Fig. 3. The charge distribution of the (a), (b) Z-PCMI and (c), (d) Z-PCMS at the resonant wavelengths of 1582 nm and 578 nm under the illumination of the LCP and RCP.

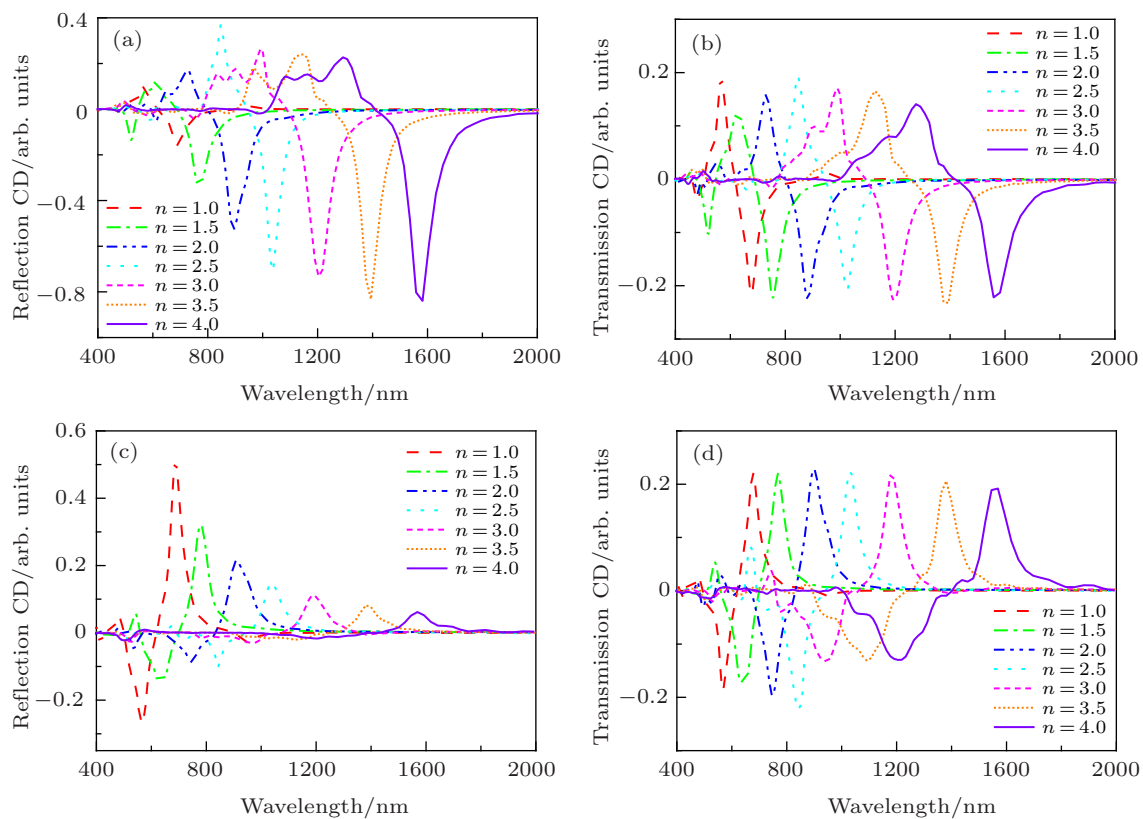


Fig. 4. The influence of the refractive index n_{top} on CD peaks. (a), (b) The reflection CD_R and transmission CD_T intensities of the Z-PCMI for the light illuminating along $-Z$ direction. (c), (d) The reflection CD_R and transmission CD_T intensities of the Z-PCMI for the light illuminating along $+Z$ direction.

Then, the transmission and reflection intensities of the Z-PCMI are discussed as shown in Fig. 5. For the Z-PCMI, the conversion parts of the reflection coefficient are equal to each other, i.e., $R_{+-} = R_{-+}$, and an obvious difference is observed in the non-conversion parts, i.e., $R_{++} \neq R_{--}$, as shown in Figs. 5(a), 5(c), and 5(e). When the refractive index n_{top} increases, the normal reflection parts, i.e., R_{+-} and R_{-+} , are near zero, and the difference between the non-conversion parts gradually increases, resulting in enhanced reflection CD_R . In the transmission coefficient, the non-conversion parts are equal to each other, i.e., $T_{++} = T_{--}$, and the transmission CD_T is originated from the difference between T_{+-} and T_{-+} . When the refractive index n_{top} increases, the difference between the conversion parts, i.e., T_{+-} and T_{-+} , changes a little and the non-conversion parts are not zero. Therefore, the enhancement of the reflection CD_R comes from the increase in the difference of the non-conversion components.

The simulation results show that when the linear po-

larization light illuminates along $-Z$ direction, the interface impedance and reflection coefficients increase with the increase of refractive index n_{top} . According to Eq. (3), the difference between R_{++} and R_{--} comes from the off-diagonal elements, i.e., r_{xy} and r_{yx} , of the linear reflection coefficients. The dispersion relation of the conversion parts (r_{xy} and r_{yx}) is calculated by changing the refractive index n_{top} , as shown in Fig. 6. As shown in Figs. 6(a)–6(c), when the linear polarization light illuminates along $-Z$ direction, the reflection coefficients r_{xy} and r_{yx} increase with the increase of refractive index n_{top} , resulting in the increased difference of R_{++} and R_{--} . Therefore, the large CD_R results from the increase of the reflection coefficients (r_{xy} and r_{yx}) caused by the increase of the refractive index n_{top} . When the linear polarization light illuminates along $+Z$ direction, the reflection coefficients (r_{xy} and r_{yx}) decrease with the increase of refractive index n_{top} , as shown in Figs. 6(d)–6(f). The decrease of the reflection coefficient will cause the decrease of CD_R .

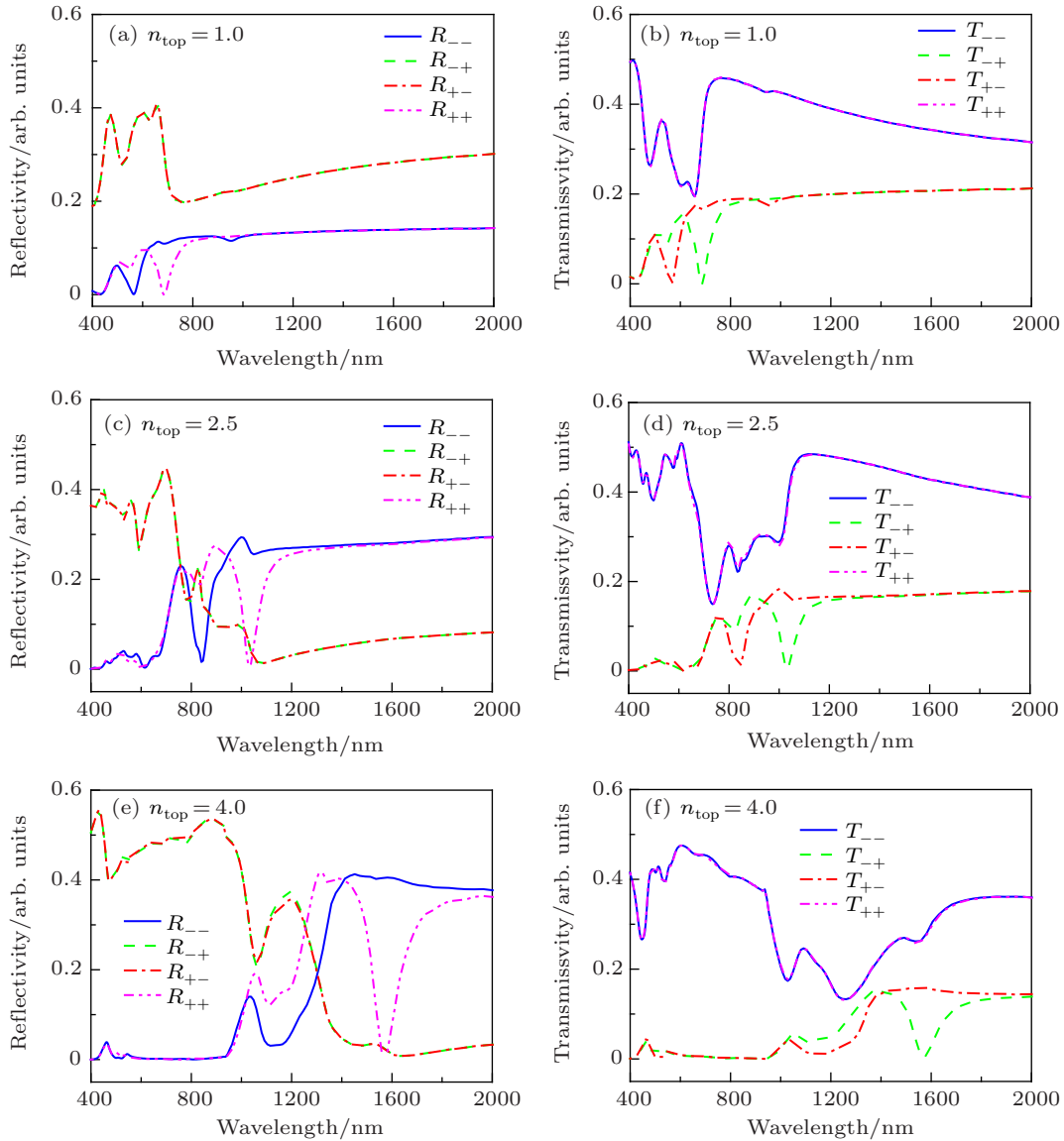


Fig. 5. (a), (c), (e) The reflection intensities and (b), (d), (f) transmission intensities of the Z-PCMI. The reflection and transmission intensities are obtained for the light illuminating along $-Z$ direction.

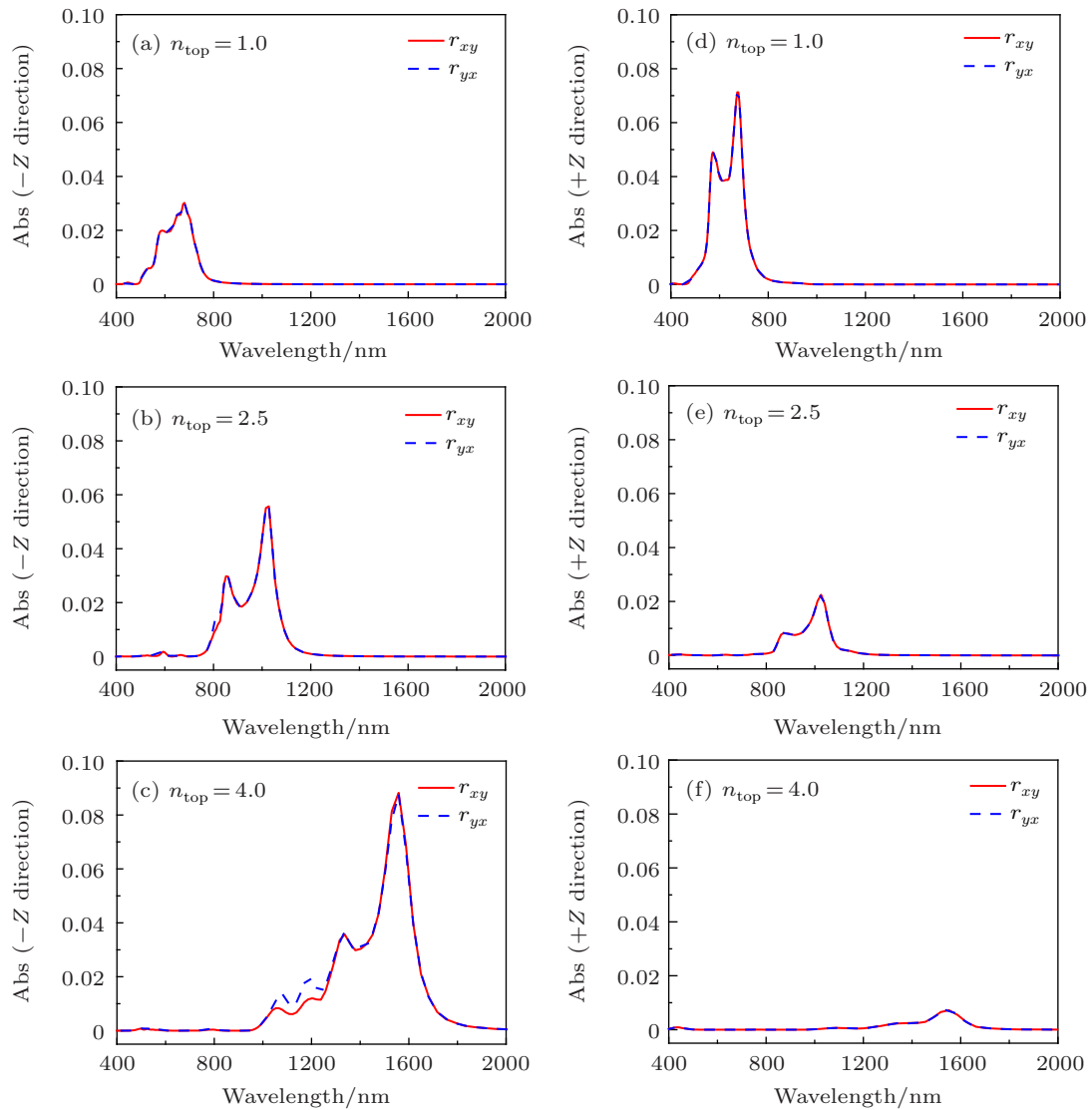


Fig. 6. The dispersion relation of the off-diagonal elements (r_{xy} and r_{yx}) of the linear reflection coefficients. (a)–(c) The linear polarization light illuminates the Z-PCMI along $-Z$ direction. (d)–(f) The linear polarization light illuminates the Z-PCMI along $+Z$ direction.

For a better comparative study, the PCMIs, which are composed of the Ag-metal-grating structure (i.e., G-PCMI) and the $\perp\perp$ -shaped structure (i.e., $\perp\perp$ -PCMI), i.e., planar isotropic achiral metamaterials and planar isotropic chiral metamaterials, are shown in Figs. 7(a) and 7(b). The lattice sizes of the chiral nanostructure array in X - and Y -directions are P_x and P_y , respectively. For the Ag-metal-grating nanostructure, the width and length are W_3 and L_3 . For the $\perp\perp$ -shaped structure, the total side length, the arm length and width are W_4 , L_4 , and L_5 . The thickness h for both of the Ag-metal-grating and $\perp\perp$ -shaped chiral nanostructures is 40 nm.

The reflection coefficients of the G-PCMI and $\perp\perp$ -PCMI are shown in Figs. 7(c), 7(e), 7(g) and 7(d), 7(f), 7(h), respectively. For the G-PCMI, the conversion, i.e., R_{+-} and R_{-+} , and non-conversion parts, i.e., R_{++} and R_{--} , are equal to each other. The conversion parts gradually increase and the non-conversion parts approach to zero. When the refractive index n_{top} increases, the difference between the conversion parts and the non-conversion parts also gradually increases, as shown in

Figs. 7(c), 7(e), and 7(g). These results indicate that the reflection coefficients of planar isotropic achiral metamaterials are significantly related to the refractive index of the two media. For the $\perp\perp$ -PCMI, the non-conversion parts are not observed in the reflection coefficient, i.e., $R_{++} = R_{--} = 0$, and the conversion parts are also equal to each other, i.e., $R_{+-} = R_{-+}$, indicating that no CD signal is observed in the reflection as shown in Figs. 7(d), 7(f), and 7(h). However, as the refractive index n_{top} increases, the non-conversion parts are zero and the conversion parts are equal but decrease. Therefore, when the planar isotropic chiral metamaterials are placed on the interface of two media, no CD signal is observed. Three types of structures are discussed here, one is the G-PCMI, one is the $\perp\perp$ -PCMI, and the other is the Z-PCMI, only the Z-PCMI which is to place the PACMs on the interface of two media can obtain the chiroptical effect, and the large reflection CD_R is related to the large refractive index difference of the two media.

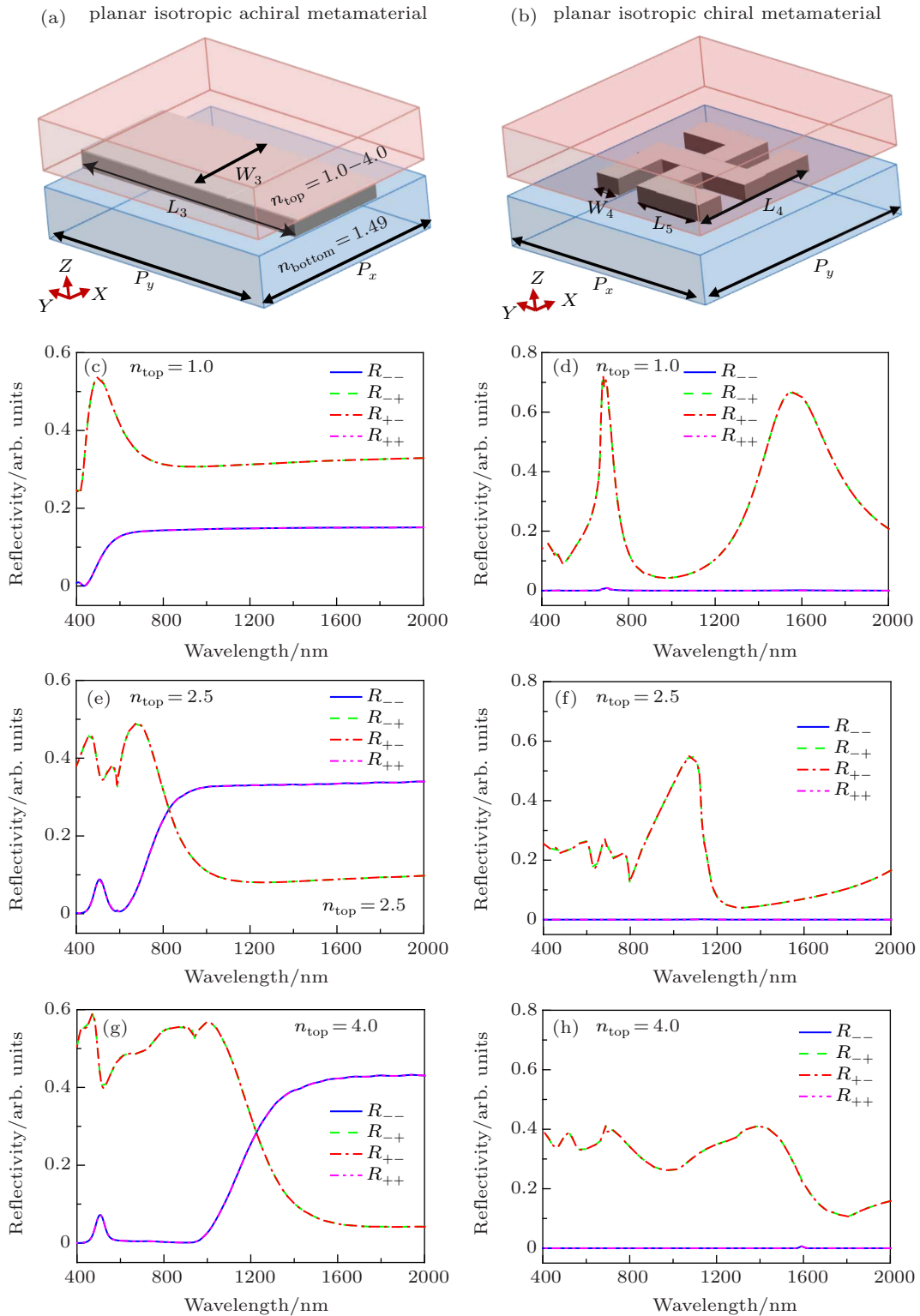


Fig. 7. The reflection intensities of the G-PCMI and $\bar{\Gamma}$ -PCMI. (a) Schematic diagram of the G-PCMI, the structure parameters are set as $W_3 = 115$ nm, $L_3 = 335$ nm, $P_x = 235$ nm, and $P_y = 335$ nm. (b) Schematic diagram of the $\bar{\Gamma}$ -PCMI, the structure parameters are set as $W_4 = 50$ nm, $L_4 = 250$ nm, $L_5 = 125$ nm, and $P_x = P_y = 450$ nm. The thickness h for both of the Ag-metal-grating and the $\bar{\Gamma}$ -shaped structures is 40 nm. The reflection intensities of (c), (e), (g) the G-PCMI; and (d), (f) (h) the $\bar{\Gamma}$ -PCMI. The refractive index n_{top} is increased from 1 to 4, while the refractive index n_{bottom} keeps at 1.49.

4. Conclusion

In this work, we report a simple method to enhance the reflection CD_R by placing the PACMs on the interface of two media. In simulations, two types of structures have been investigated, one is the Z-PCMI that places the Z-shaped PACMs on

the interface of two media, and the other is the Z-PCMS that places the Z-shaped PACMs directly on the substrate. Simulation results indicate that for the Z-PCMS, only a weakly reflection CD_R signal is observed no matter what the refractive index difference of the two media is. While for the Z-PCMI, a

large chiroptical effect can be observed by changing the refractive index difference. And the maximum and minimum reflection CD_R from the Z-PCMI can reach about 0.840 and 0.157, respectively, resulting in a large available range of reflection CD_R from -0.840 to -0.157 . Meanwhile, the transmission CD_T remains unchanged when changing the refractive index difference of the two media. Further research on three types of structures (i.e., G-PCMI, Π -PCMI, and Z-PCMI) indicates that the reflection CD_R is derived from the difference of the non-conversion components of the PACMs, and a large reflection CD_R is related to the refractive index difference of the two media. Our results provide a simple approach to enhance the chiroptical response and can be used in various fields, such as biosensing, circular polarizer, chiral catalysis, and chiral photo detection.

References

- [1] Pagès S, Lagugné-Labarthe F, Buffeteau T and Sourisseau C 2002 *Appl. Phys. B* **75** 541
- [2] Wang L, Huang X, Li M and Dong J 2019 *Opt. Express* **27** 25983
- [3] Turner M D, Saba M, Zhang Q, Cumming B P, Schröder-Turk G E and Gu M 2013 *Nat. Photon.* **7** 801
- [4] Eidelstein G, Fardian-Melamed N, Gutkin V, Basmanov D and Kotlyar A 2016 *Adv. Mater.* **28** 4944
- [5] Liu Y and Zhao X 2018 *Chin. Phys. B* **27** 117805
- [6] Gansel J K, Thiel M, Rill M S, Decker M, Bade K, Saile V, Freymann G V, Linden S and Wegener M 2009 *Science* **325** 1513
- [7] Kuwata-Gonokami M, Saito N, Ino Y, Kauranen M and Svirko Y 2005 *Phys. Rev. Lett.* **95** 227401
- [8] Chen W, Abeyasinghe D C, Nelson R L and Zhan Q 2010 *Nano Lett.* **10** 2075
- [9] Jiang S C, Xiong X, Hu Y S, Hu Y H, Ma G B, Peng R W, Sun C and Wang M 2014 *Phys. Rev. X* **4** 021026
- [10] Wang J, Tian H, Li S, Li L, Wang G, Gao J, Guo W and Zhou Z 2020 *Opt. Lett.* **45** 1276
- [11] Lee S J and Lin W 2002 *J. Am. Chem. Soc.* **124** 4554
- [12] Anker J N, Hall W P, Lyandres O, Shah N C, Zhao J and Van Duyne R P 2008 *Nat. Mater.* **7** 442
- [13] Zhang S, Park Y S, Li J, Lu X, Zhang W and Zhang X 2009 *Phys. Rev. Lett.* **102** 023901
- [14] Hoffman A J, Alekseyev L, Howard S S, Franz K J, Wasserman D, Podolskiy V A, Narimanov E E, Sivo D L and Gmachl C F 2007 *Nat. Mater.* **6** 946
- [15] Plum E, Zhou J, Dong J, Fedotov V A, Koschny T, Soukoulis C M and Zheludev N I 2009 *Phys. Rev. B* **79** 035407
- [16] Zhao R, Zhou J, Koschny T, Economou E N and Soukoulis C M 2009 *Phys. Rev. Lett.* **103** 103602
- [17] Zhao R, Koschny T, Economou E N and Soukoulis C M 2010 *Phys. Rev. B* **81** 235126
- [18] Cao T, Wei C, Mao L and Li Y 2014 *Sci. Rep.* **4** 7442
- [19] Cheng Y Z, Chen F and Luo H 2020 *Phys. Lett. A* **384** 126398
- [20] Tang M, Zhou X X, Luo H L and Wen S C 2012 *Chin. Phys. B* **21** 124201
- [21] Wang H and Zhang X 2011 *Phys. Rev. A* **83** 053820
- [22] Fedotov V A, Mladonov P L, Prosvirnin S L, Rogacheva A V, Chen Y and Zheludev N I 2006 *Phys. Rev. Lett.* **97** 167401
- [23] Cheng Y Z, Yang Y L, Zhou Y J, Zhang Z, Mao X S and Gong R Z 2016 *J. Mod. Opt.* **63** 1675
- [24] Decker M, Zhao R, Soukoulis C M, Linden S and Wegener M 2010 *Opt. Lett.* **35** 1593
- [25] Cheng Y Z, Gong R Z and Wu L 2016 *Plasmonics* **12** 1113
- [26] Liu D Y, Luo X Y, Liu J J and Dong J F 2013 *Chin. Phys. B* **22** 124202
- [27] Kaschke J, Gansel J K and Wegener M M 2012 *Opt. Express* **20** 26012
- [28] Cui Y, Kang L, Lan S, Rodrigues S and Cai W 2014 *Nano Lett.* **14** 1021
- [29] Rehman M U, Hua C and Lu Y 2020 *Chin. Phys. B* **29** 057304
- [30] Frank B, Yin X, Schäferling M, Zhao J, Hein S M, Braun P V and Giessen H 2013 *ACS Nano* **7** 6321
- [31] Lesot P and Lafon O 2008 *Chem. Phys. Lett.* **458** 219
- [32] Heng H and Wang R 2016 *Chin. Phys. Lett.* **33** 53
- [33] Yang X, Li M, Hou Y D, Du J L and Gao F H 2019 *Opt. Express* **27** 6801
- [34] Menzel C, Rockstuhl C and Lederer F 2010 *Phys. Rev. A* **82** 053811
- [35] Menzel C, Helgert C, Rockstuhl C, Kley E, Tunnermann A, Pertsch T and Lederer F 2010 *Phys. Rev. Lett.* **104** 253902
- [36] Georgieva E 1995 *J. Opt. Soc. Am. A* **12** 2203
- [37] Cheng Q and Cui T J 2007 *J. Opt. Soc. Am. A* **23** 3203
- [38] Lu Y F and Han Y P 2019 *Chin. Phys. B* **28** 024202
- [39] Ghaffar A and Alkanhal Majeed A.S. 2015 *Int. J. Appl. Electrom.* **47** 805
- [40] Li W, Coppens Z J, Besteiro L V, Wang W, Govorov A O and Valentine J 2015 *Nat. Commun.* **6** 8379